Full-scale fire test on an earthquake-damaged reinforced concrete frame

Fire Safety Journal 73 (2015) 1–19

Contents lists available at ScienceDirect

Fire Safety Journal

journal homepage: www.elsevier.com/locate/firesaf

Full-scale fire test on an earthquake-damaged reinforced concrete frame

Praveen Kamath [a], Umesh Kumar Sharma [a,*], Virendra Kumar [b], Pradeep Bhargava [a], Asif Usmani [c], Bhupinder Singh [a], Yogendra Singh [d], Jose Torero [e], Martin Gillie [f], Pankaj Pankaj [c]

[a] Department of Civil Engineering, Indian Institute of Technology Roorkee, Roorkee 247667, India
[b] Department of Civil Engineering, National Institute of Technology Jamshedpur, Jamshedpur 831014, India
[c] Institute for Infrastructure and Environment, School of Engineering, University of Edinburgh, Edinburgh EH9 3JL, UK
[d] Department of Earthquake Engineering, Indian Institute of Technology Roorkee, Roorkee 247667, India
[e] School of Civil Engineering, University of Queensland, Queensland 4072, Australia
[f] School of Mechanical, Aerospace and Civil Engineering, University of Manchester, Manchester M60 1QD, UK

ARTICLE INFO

Article history:
Received 26 August 2012
Received in revised form
12 December 2014
Accepted 1 February 2015

Keywords:
Post earthquake fire
Reinforced concrete frame
Full-scale testing and structural performance

ABSTRACT

Fire, in the aftermath of an earthquake has evolved as a severely destructive force since the last century [1]. Codes and regulations exist in countries situated in seismically active regions of the world in order to ensure safety of buildings and their occupants in the event of an earthquake; it is however rare to find regulations that also require the consideration of fire following an earthquake, thereby leaving this possibility to be dealt with entirely by emergency responders on an ad-hoc basis with little preparedness. Fire following earthquake (FFE) events in the past, although rare, have sometimes been as destructive as the original earthquake. The aim of this study was to carry out a set of full-scale loading tests on an earthquake damaged, reinforced concrete frame subsequently exposed to fire. The sequential loading was devised in the form of a three phase testing procedure – simulated earthquake loading facilitated by cyclic quasi-static lateral loads; followed by a compartment fire; and finally by subjecting the earthquake and fire damaged frame to a monotonic pushover loading to assess its residual capacity. The reinforced concrete frame was well instrumented with numerous sensors, consisting of thermocouples, strain gauges, linear variable differential transducers (LVDTs) and pressure sensors. A large database of results consisting of temperature profiles, displacements and strains has been generated and salient observations have been made during each stage of loading. This paper describes the experimental investigation and serves as a vehicle for dissemination of the key findings and all the important test data to the engineering community which could be used for validating numerical simulations for further advancing the knowledge and understanding in this relatively poorly researched area.

1. Introduction

The risk of fires in the aftermath of earthquakes is well known. Two largest peacetime fire disasters, regarded as the worst ever fire disasters for mankind in the twentieth century: San Francisco (1906) and Tokyo (1923) were essentially triggered by earthquakes. Major conflagrations and widespread devastation were reported in both the events resulting in far greater damage attributed to the fires than that caused by the earthquakes on their own. In the 1906 San Francisco earthquake and fire, about 28,000 buildings were destroyed whereas in 1923 earthquake and fire, about 447,000 houses were destroyed by the blazing fire. The majority of buildings those days were constructed using timber. The modern cities of San Francisco and Tokyo are completely surrounded with reinforced concrete (RC) tall buildings and structures. Fortunately, the scales of these events have not been repeated; though there have been many major earthquakes, which have led to fires in their wake. Nearly all major Californian earthquakes were followed by multiple ignitions, most notably the 1989 Loma Prieta and the 1994 Northridge earthquakes, both of which were followed by over 100 ignitions each. After the 1995 Hanshin, Kobe (Japan) earthquake, over 100 ignitions were recorded in Kobe City. The 1999 earthquake of Marmara (Turkey) was followed by many local fires in buildings and industrial premises which were classified as uncontrollable. Collapse of reinforced concrete structures were predominantly reported in the

* Corresponding author. Fax: +91 1332 275568.
E-mail address: umuksh@rediffmail.com (U.K. Sharma).

http://dx.doi.org/10.1016/j.firesaf.2015.02.013
0379-7112/

two latter fire following earthquake (FFE) events. In the 1995 Hanshin FFE event, a 90 m high RC heater stack collapsed whereas in the 1999 Marmara FFE event, many mid-rise non-ductile RC frames were reported to be damaged in the earthquake and further affected by fire [2]. It is also important to note that many recent earthquakes, viz., Haiti (2010), Fukushima (2011) and Chile (2014) were followed by many conflagrations that damaged lifelines and critical facilities such as hospitals, oil refineries, and city

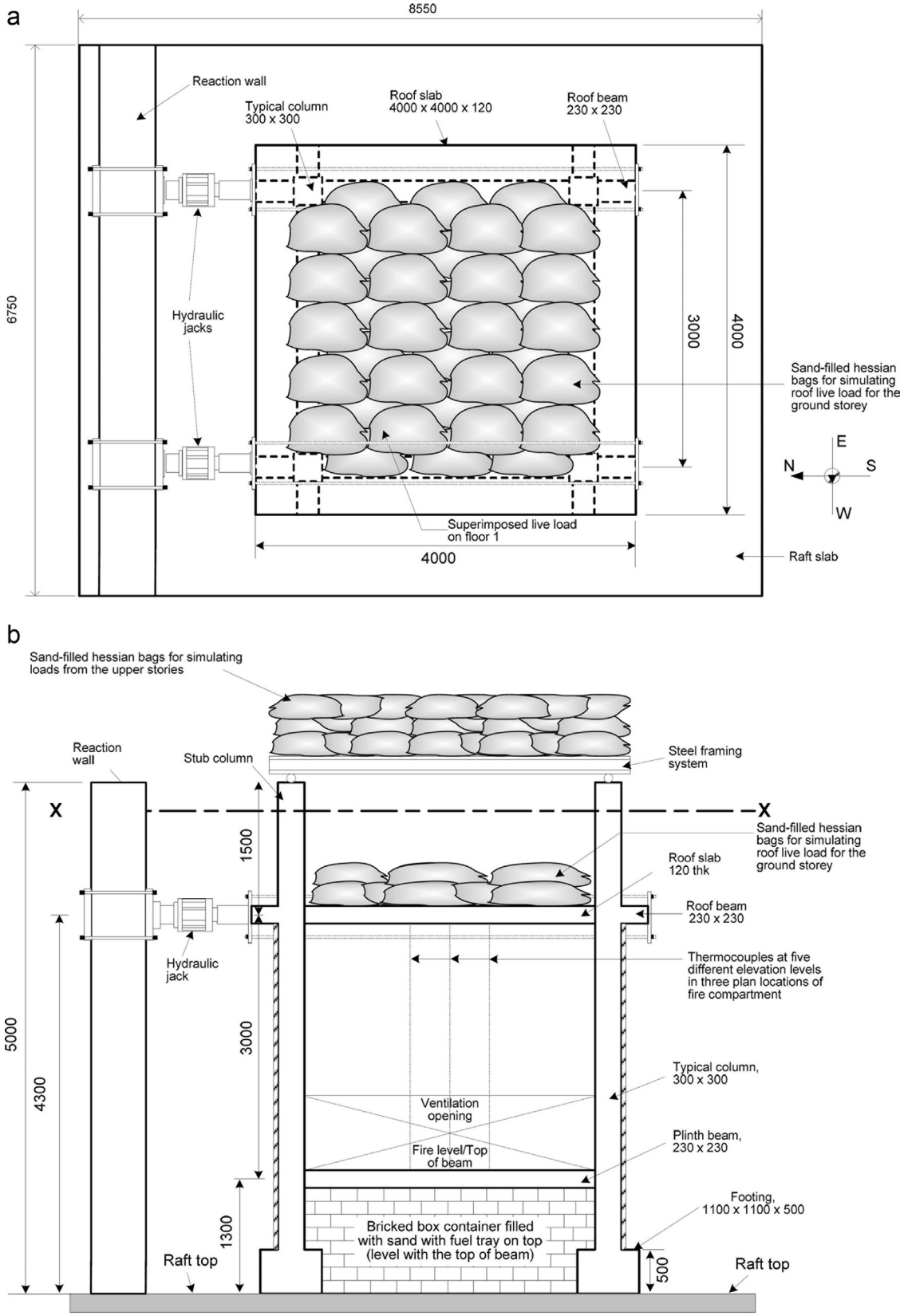

Fig. 1. Schematic of the test setup (a) plan and (b) elevation.

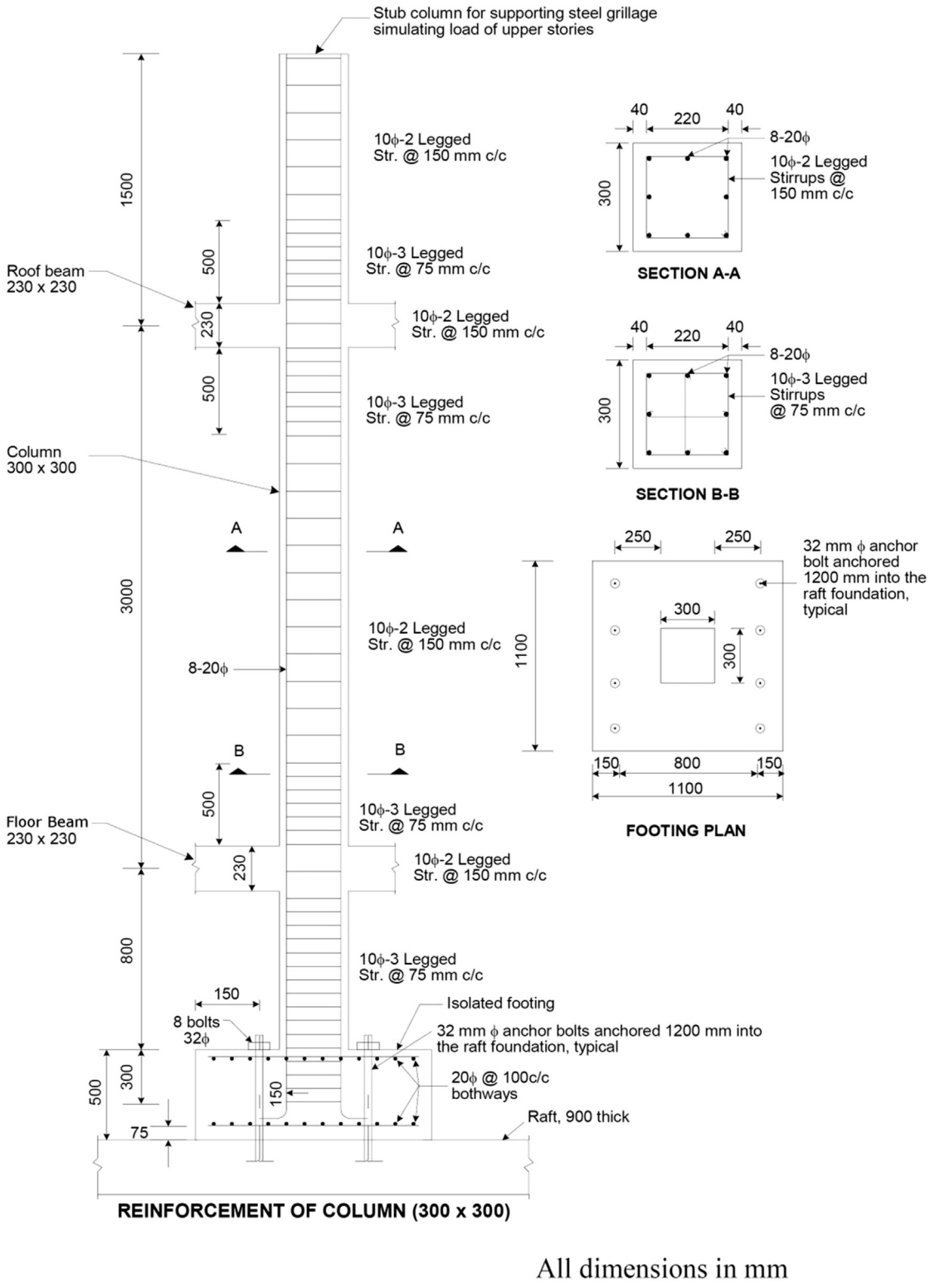

Fig. 2. Detailing of a typical column per IS 13920:1993.

centre areas irrespective of their type of construction [3–5]. Other sources of fires included outbreak of forest fires in earthquake hit zones, viz., Chile, where as many as 2000 houses in the densely populated areas were destroyed [6]. The level of urbanisation and industrialisation and improper storage and disposal of HAZMATs in seismic zones are obvious factors that exacerbate the risks associated with FFE events.

Building codes in most countries require engineers to consider the effect of seismic and fire loading on structures in order to provide an adequate level of resistance to these hazards, however this is done on a separate basis without considering any linkage between the two hazards. There are no current regulations that

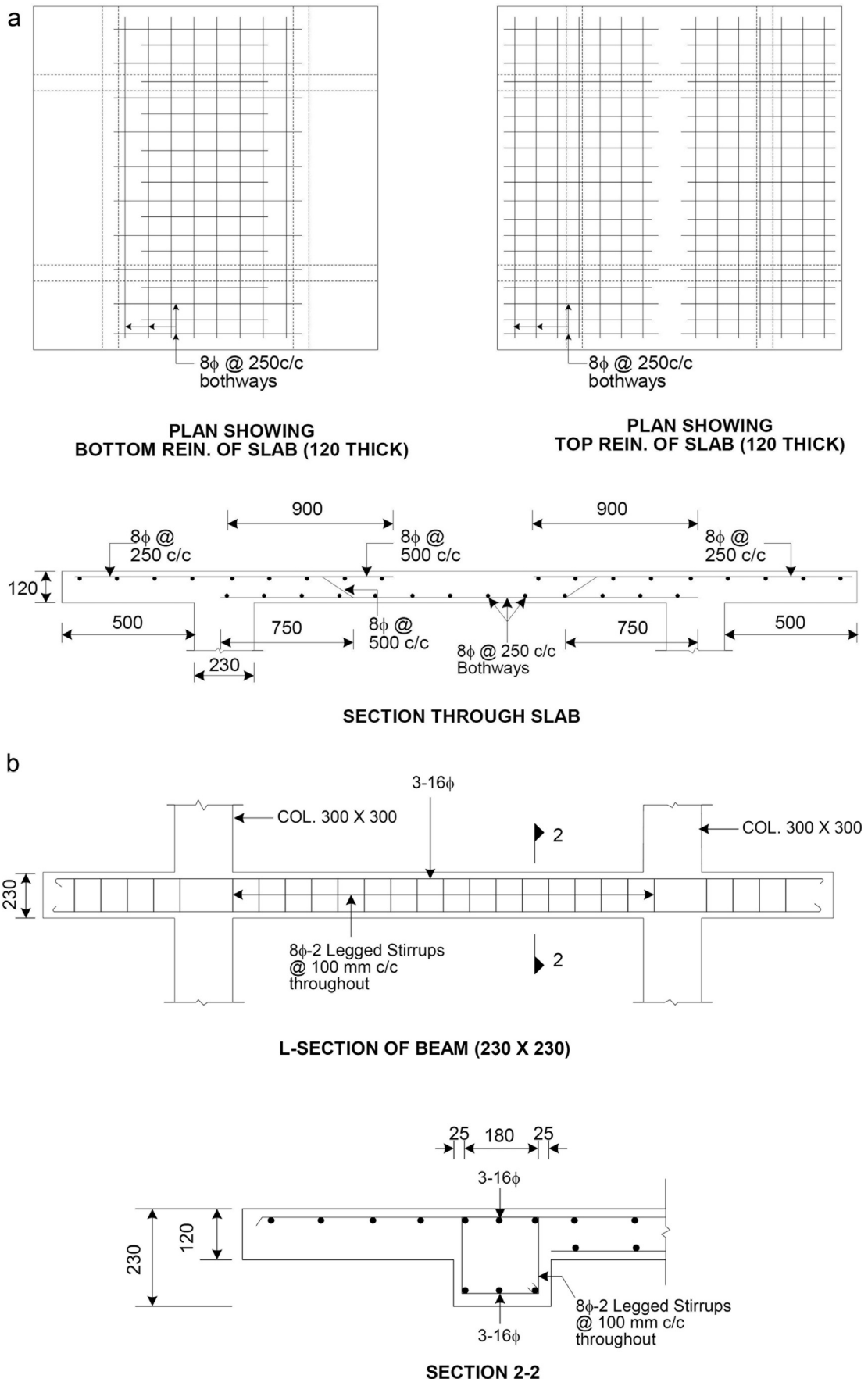

Fig. 3. Detailing of reinforcement in a typical (a) slab and (b) beam.

Table 1
Mechanical properties of the steel reinforcement under ambient conditions.

Dia of steel rebar and usage	Yield stress (MPa)	Ultimate stress (MPa)	Yield strain (mm/mm)	Ultimate strain (mm/mm)	Elongation (%)	Young's modulus ($\times 10^5$ MPa)
8 mm (Slab and beam ties)	550.69	642.97	0.0047	0.2070	20.7	2.14
10 mm (Column ties)	446.57	538.21	0.0042	0.1960	19.6	2.13
16 mm (Beam main reinforcement)	420.05	541.18	0.0023	0.1689	16.89	2.03
20 mm (Column main reinforcement)	448.55	567.50	0.0021	0.1458	14.58	2.10

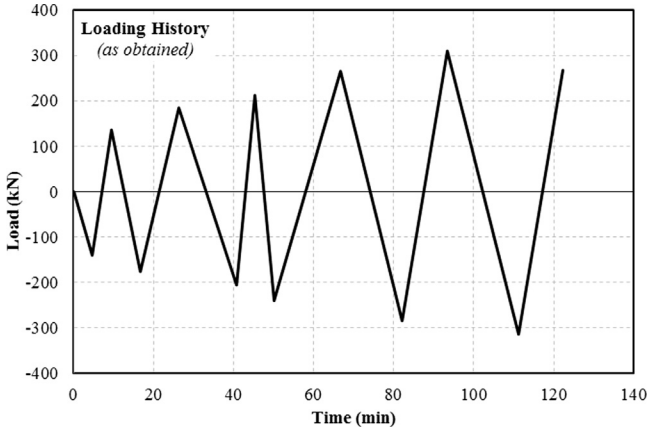

Fig. 4. Loading history of the test frame (*as obtained*).

require structures to consider these hazards in a sequential manner and neither is there any available quantification of such compound loading, using which could assist engineers in providing structures with the required resistance if desirable from a performance perspective. A critical review of the literature shows that research on behaviour of concrete structures under post-earthquake fires is still in its infancy. Considerable new research effort in the form of full-scale tests is required for addressing the challenges posed by FFE in order to generate the requisite understanding and its quantification. Although some of this type of work has been discussed in earlier literature [7], to the best of the authors' knowledge no experimental studies have been conducted previously for reckoning the structural response of an RC frame under a FFE event. A full-scale test involving the investigation of the fire performance of 5 storey RC building damaged by inducing ground motion on a shake table was performed at University of California San Diego's outdoor test facility. However, the scope of the test was limited to the aspects of building fire safety, namely compartmentation, performance of fire protection systems, fire-stop systems, performance of exterior façade in relation to the escape of fire and smoke and fire and smoke transmission though the interior [8].

In view of the preceding discussion, the primary objective of the study undertaken in this research was to examine experimentally the performance of a typical reinforced concrete building frame under an FFE scenario. The sequential loading consisted of first subjecting the RC test frame to cyclic quasi-static loading against a reaction wall in a dedicated outdoor testing facility at the Department of Civil Engineering, Indian Institute of Technology Roorkee so as to induce a pre-defined seismic damage. The damaged test frame was then exposed to a one hour compartment fire fed by a pool of kerosene.

2. Experimental programme

A single storey RC test frame was constructed on the strong floor of the test facility, which forms the test frame of the present investigation. The test setup in plan and elevation is presented in Fig. 1(a) and (b), respectively, which also shows the geometric dimensions of the test frame. The test frame consisted of four 300 mm square columns at 3000 mm centres in the N–S and E–W directions supporting a grid of four 230×230 mm^2 beams underlying a 120 mm thick RC roof slab as shown in Fig. 1(b). The hydraulic jacks were located in the north direction and the ventilation opening for the fire compartment was facing the west direction as shown in Fig. 1(a). Plinth beams (used in India for supporting masonry walls above ground level) also known as grade beam were also provided at the level of the ground floor and their size and configuration were similar to the roof beams of the building. All the elements of the test frame were cast in different concrete lifts. Column fixity at the base was provided by the termination of all the four columns into a 900 mm thick RC raft foundation of plan size 6750×8550 mm^2. The building frame was designed according to the recommendations of the relevant Indian Standards. The ductile design of the test frame was established based on the recommendations of IS 13920 [9] and the typical detailing of the reinforcement in the column, slab and beam of the test frame are shown in Figs. 2 and 3(a, b), respectively. They satisfy the requirements of IS 13920 [9] and SP: 34 [10]. Although it is desirable to use nominally identical companion specimens in any structural testing programme to ensure repeatability of test results, because of the nature of test and resource constraints only one frame was tested.

The test frame was supported on the raft of the strong-floor and reaction wall testing facility built specifically for this purpose. The casting of the test frame occurred in five stages. The pedestals were cast first on the strong-floor followed by the casting of 800 mm height of the columns up to the soffit of the plinth beams. The plinth beams were then cast together with 300 mm height of columns, which was followed by the construction of 1500 mm height of all the columns. The rest of the frame was cast in one go during the last pour of concrete in the structure. Care was taken in the treatment of cold joints in the building to ensure that the different segments of the concreted structure were properly bonded to each other. Care was also taken during mixing and placing operations to ensure consistent concrete properties and consolidation. Sufficient number of control specimens according to the requirements of the Indian concrete code IS 456 [11] were collected to monitor strength development in the test frame, particularly for determining the strength of concrete in the frame at the time of testing.

2.1. Materials

The mixture proportions of concrete used for casting the various elements of the frame were in the proportion of 1:1.23:2.70, representing cement, fine aggregate and coarse aggregate respectively with a water–cement ratio of 0.44. The equivalent mean cube compressive strength of concrete was 33.6 Mpa on the day of the test. The compressive strength was estimated according to the Indian Code IS456:2000 [11] based on 9 cubes (3 cubes per concrete pour), the strengths of which were in the range of $\pm$ 15% of

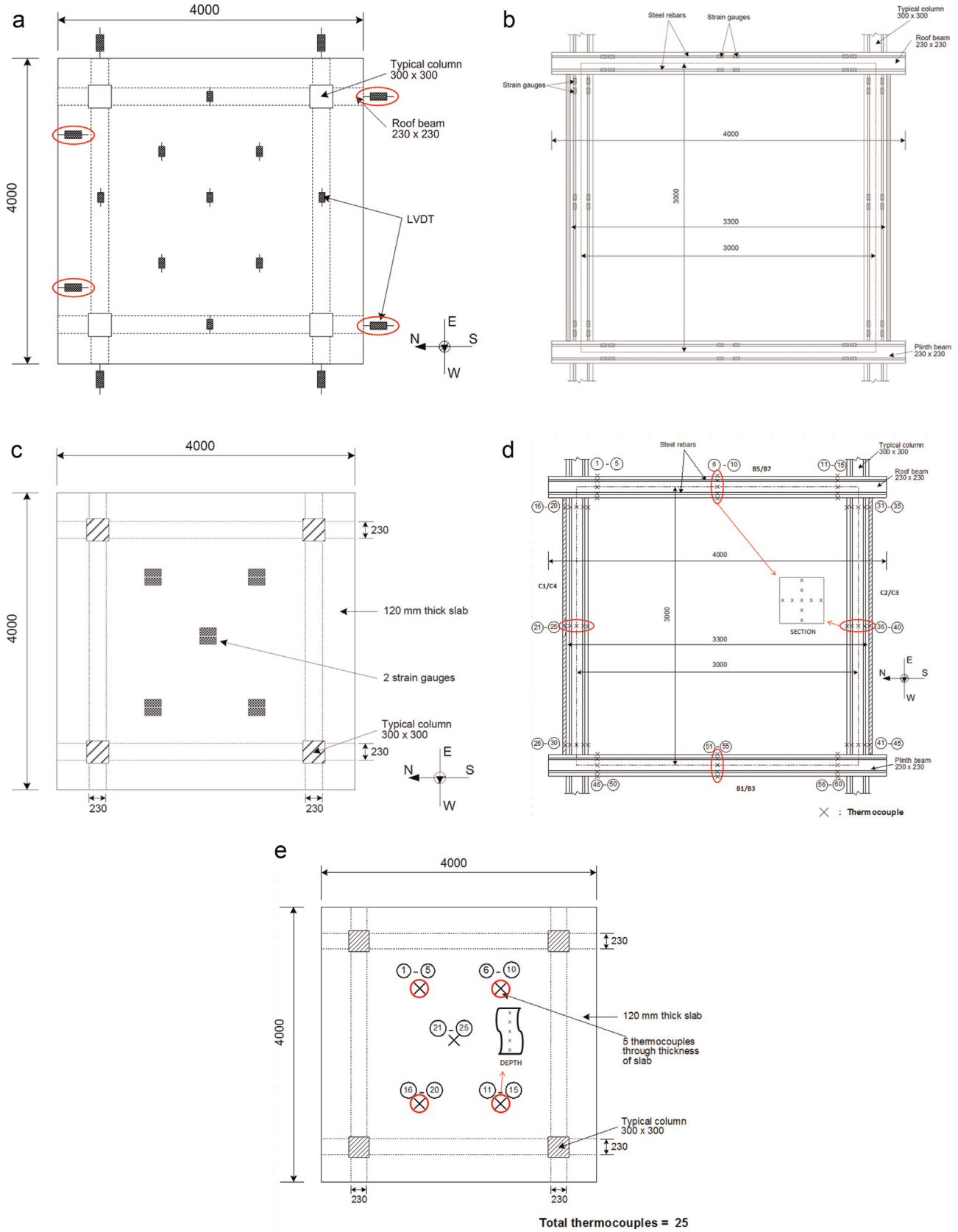

Fig. 5. Instrumentation of the RC test frame (a) LVDT, (b) strain gauges (*in beams and columns*) (c) strain gauges (*in slab*), (d) thermocouples (*in beams and columns*), and (e) thermocouples (*in slab*).

Fig. 6. (a) Simulated earthquake loading, (b) fire test and (c) residual capacity test on fire damaged RC frame.

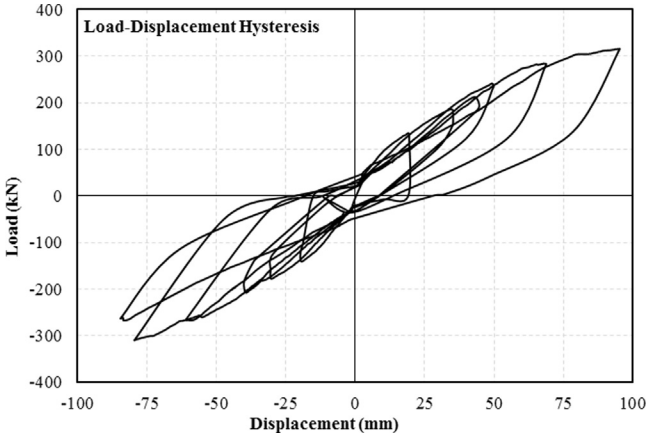

Fig. 7. Load–displacement hysteretic curve.

the mean strength reported. The details of the steel reinforcement used and its mechanical properties are provided in Table 1. Concrete mix-proportioning was designed according to Indian Standard IS10262:2009 [12] and the concrete was produced in accordance with IS456:2000 [11]. A needle vibrator was used to ensure proper compaction of the green concrete in casting all the test frame components.

2.2. Key stages of the experiment

The following sections describe the stages of the test, namely application of gravity loading; cyclic lateral loading to simulate seismic damage; fire following the simulated seismic damage; and a residual lateral load capacity test of the damaged and fire exposed frame after it had cooled down to the ambient environment temperature.

2.2.1. Gravity loading

A platform made of orthogonally oriented rolled steel I-beams was constructed to rest on the four columns protruding above the roof slab of the test frame. This platform was loaded with 1 m × 1 m × 0.1 m precast concrete slab strips and sand-filled hessian bags. The gravity loading was based on assuming that the test frame columns were supporting the load of three stories above the ground floor in a notional R.C. building. According to the recommendations of the Indian seismic design code, IS 1893 (Part-1) [13], only 25% of the assumed uniformly distributed floor live

Fig. 8. Nomenclature for the identification of RC test frame members and schematic of cracks due to cyclic loading.

(or imposed) load of 2 kN/m^2 is considered for seismic weight calculations. Therefore, for estimating the loading on the platform the full complement of the dead load and 25% of the live load from the assumed upper floors was considered, making a total gravity load of approximately 400 kN on the test frame. A schematic of gravity loads on the loading platform is shown in Fig. 1(a) and (b).

2.2.2. Simulated seismic lateral loading

Cyclic lateral loads on the test frame were applied in a quasi-static manner in load-controlled mode using a pair of double

Table 2
Formation of cracks in the RC test frame under cyclic loading.

Structural member	Crack no.	Roof slab displacement and loading direction
Slab	1	69 mm N–S
B5	2	50 mm N–S
B5	3, 4	80 mm S–N
B5	1	95 mm N–S
B7	1, 2	35 mm S–N
B7	3	95 mm N–S
C1	6, 9	31 mm N–S
C1	7, 8	35 mm S–N
C1	4, 5	95 mm N-S
C1	1, 2, 3	85 mm S–N
C2	9, 10, 11, 12, 13, 14	35 mm S–N
C2	1, 2, 3	85 mm S–N
C2	5, 6, 7	95 mm N–S
C2	4, 8	85 mm S–N
C3	9	31 mm N–S
C3	1, 2, 3, 4	80 mm S–N
C3	5, 6	95 mm N–S
C3	7, 8	85 mm S–N
C4	1, 3	69 mm N-S
C4	2, 4	80 mm S–N
C4	5, 7	95 mm N–S
C4	6	85 mm S–N
B1	4, 5, 6	40 mm N–S
B1	2, 3	44 mm S–N
B1	8, 9	61 mm S–N
B1	7, 10, 11	69 mm N–S
B1	1	80 mm S–N
B3	8	31 mm N–S
B3	3	35 mm S–N
B3	4, 6	40 mm N–S
B3	2, 7	44 mm S–N
B3	5, 9	95 mm N–S
B3	1	85 mm S–N

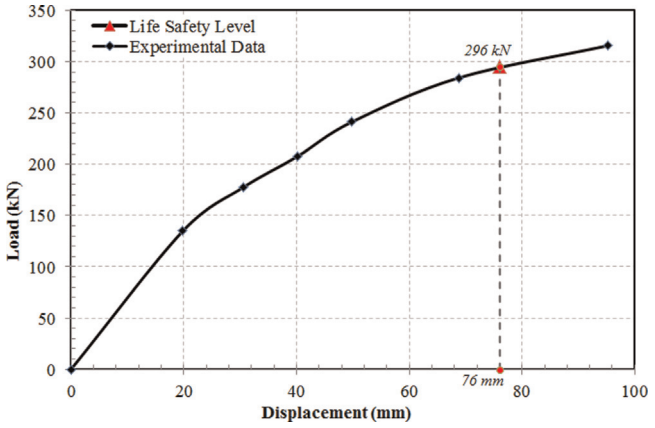

Fig. 9. Base shear vs. roof displacement.

acting hydraulic rams acting in tandem with each other against a stiff reaction wall and loading the frame at the roof slab level. The simulated seismic pre-damage thus induced corresponds to the life safety level of structural performance according to FEMA 356 [14]. The targeted lateral displacement in the first cycle of loading was 10 mm and this displacement was applied within 5 min and incremented by 10 mm in successive loading cycles so that at the conclusion of the loading cycles, the test frame was subjected to a pre-calculated maximum displacement in order to induce the desired level of mechanical damage. The loading history of the RC test frame obtained by inducing lateral displacement corresponding to the life safety level of structural performance is presented in Fig. 4. The calculated maximum target lateral displacement of the test frame at roof level was 76 mm, which corresponds to an inter-storey drift ratio of 2% (Table C1-3, FEMA 356 [14]). However, since the process was load controlled, the maximum lateral displacement obtained was ~95 mm. This behaviour is attributed to the process where an attempt was made to maintain a constant load for facilitating the crack mapping activity. To ensure quasi-static loading, a time interval of about 300 s (frequency of 0.0033 Hz) [15] was chosen. However, upon loading, a constant time interval could not be followed due to the limitations of manual load controller attached to the hydraulic jacks. Also, the loading was stalled at intervals after each cycle to identify and study the growth of cracks in different members of the RC test frame.

2.2.3. Fire loading

Subsequent to the testing of RC test frame under simulated seismic load, the test frame was subjected to a compartment fire test. Before the actual fire test, a realistic compartment fire was designed and tested in three mock fire tests, which were conducted in a temporarily constructed brick masonry compartment of size 3000 mm × 3000 mm × 3000 mm as a replica of the compartment that would encapsulate the frame in the actual tests. The compartment included a 3000 mm wide and 1000 mm height opening at the base of one of its four sides. The opening was designed according to Thomas and Heselden [16] to achieve compartment temperatures in the range of 900–1000 °C using kerosene oil as fuel in a pool fire. The maximum temperatures in the range of 1198–1327 °C could be achieved in the third mock fire test after the 21st minute and thus this fire design was chosen for the fire testing of the R.C. frame.

During the actual fire test of the RC test frame, the mild steel tray burner of size 1 m × 1 m × 0.05 m was placed at the centre of the compartment as in the mock fire tests. A galvanised iron pipe of diameter 0.0254 m was used for supplying the fuel to the burner at a peak flow rate of 1.43×10^{-4} m^3/s using a fixed head. The test frame was enclosed in a compartment fabricated on site using four detachable fire-proof panels. Each panel was made of steel angles and sheets and was provided with a single layer of glass wool insulation (25.4 mm thick) as the backing material. Over this, a thick layer of insulation was provided by means of glass wool modules (300 mm × 300 mm × 200 mm in size). These modules were securely fastened to the metal frame. All panels were installed firmly around the RC test frame with one of the panels being smaller than the others to provide an identical opening as described for the mock test compartment. The supply of fuel to the tray was terminated after one hour. Thereafter the fire was allowed to burn until the fuel in the tray was exhausted. This corresponds to the decay phase, the longest of all stages of a fire.

2.2.4. Residual lateral load capacity

The final stage of the experiment comprised of subjecting the RC test frame to a monotonic pushover loading to determine its residual capacity and quantify the strength and stiffness degradation during the cyclic and fire loading stages. The RC test frame was loaded continuously by the jacks to cause a lateral displacement towards the south beyond 95 mm, the maximum displacement imposed during cyclic lateral loading stage. The loading was stopped when the hydraulic jacks reached their maximum ram length of 200 mm. The load and lateral displacement were recorded.

2.3. Instrumentation

A comprehensive instrumentation was devised for collecting the data during the simulated seismic load test and subsequently during the fire test. An on-site control room was constructed to

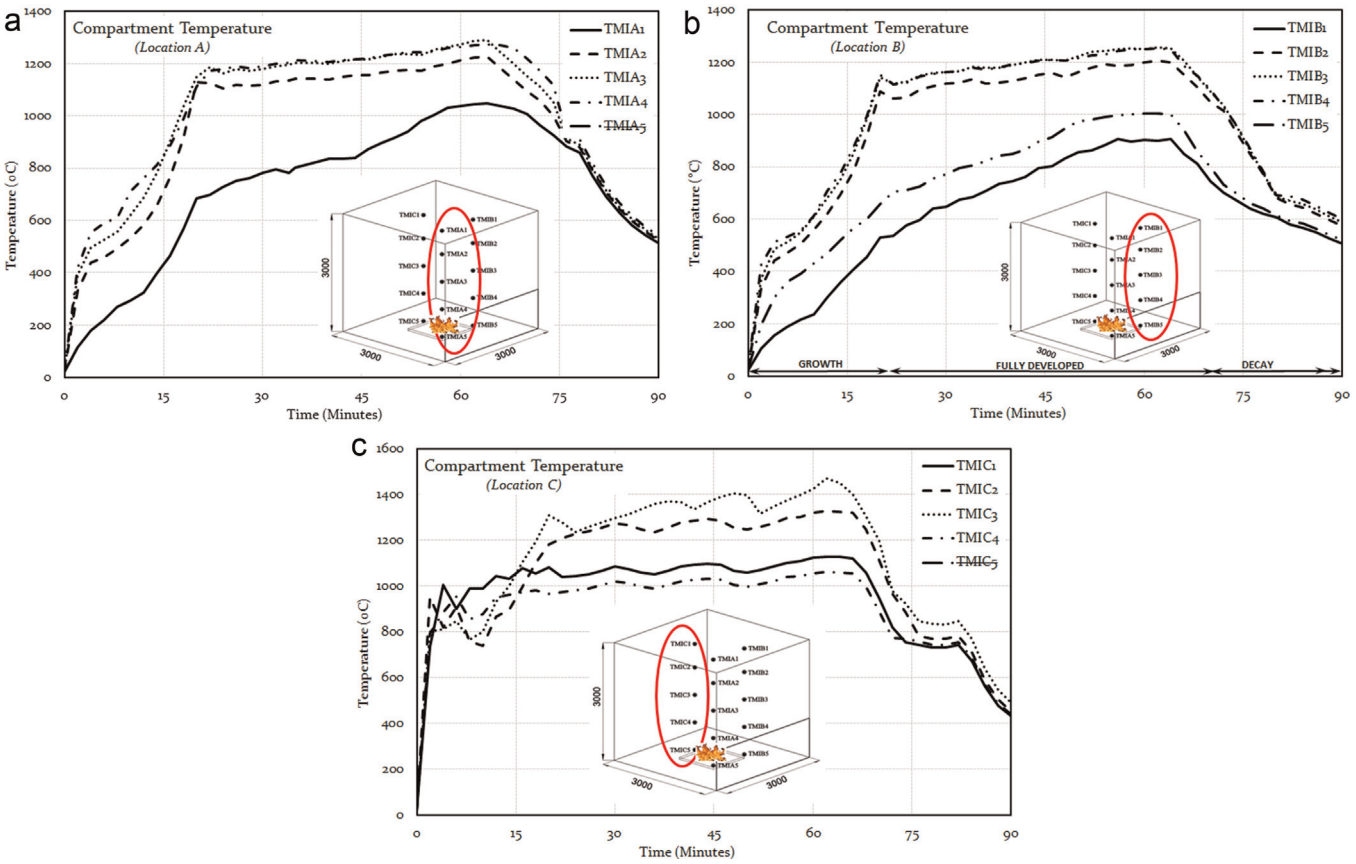

Fig. 10. Measured time–displacement curves.

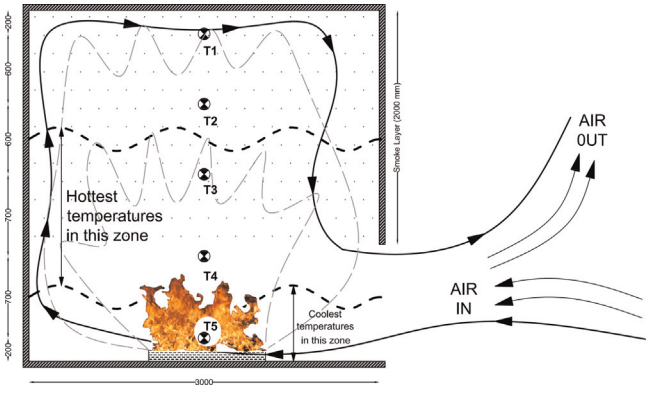

Fig. 11. Schematics of the compartment fire.

Fig. 12. Spalling in roof slab after fire.

house various data acquisition systems and workstations. The imposed cyclic lateral loads on the test frame were electronically measured using two pressure sensors mounted on each of the double-acting hydraulic rams. Displacements at the roof level were measured using a network of nine linear variable displacement transducers (LVDT), in the vertical direction and eight in the horizontal direction. Horizontal displacement transducers were positioned in both parallel and perpendicular direction against the direction of loading to capture the lateral displacement and torsion (if any). Fig. 5(a) illustrates the location of the displacement transducers at the roof level. These transducers were supported independently by a secondary frame erected on all four sides of the frame and were kept free from any localised deflections of the framed structure.

Electrical resistance-type surface mounted high temperature resistant strain-gauges were pasted on the steel rebars with the help of high temperature resistant adhesive. One hundred and six locations were chosen in roof beams, columns and slab for recording the strain patterns in the test frame. The plinth beams, which were exposed on only one face, were equipped with 48 number ambient temperature electrical-resistance type strain gauges. Fig. 5(b) and (c) shows the typical locations of strain gauges embedded inside the concrete at various key locations. The temperatures of concrete at different depths in the sections of the structural members were recorded using 0.5 mm diameter K-type thermocouples embedded along the depth and across the width as shown in Fig. 5(d). Thermocouples were installed at three different sections in the members i.e. near the end supports and at the mid-span of beams and mid-height of columns. Each section had nine thermocouples with five thermocouples along the depth of the

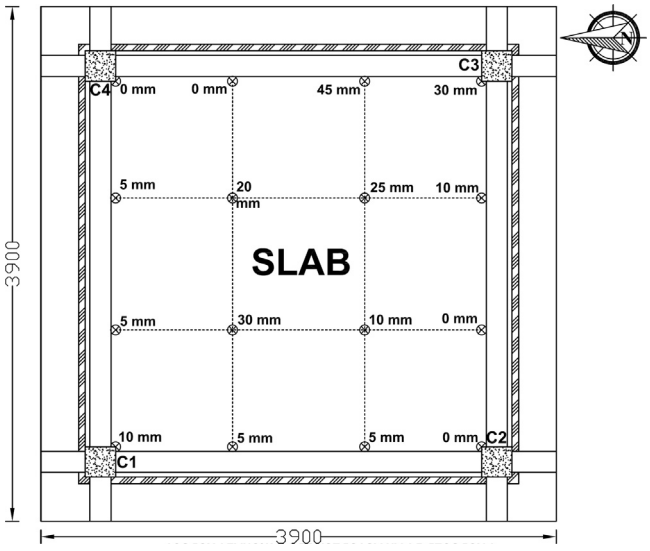

Fig. 13. Vertical residual displacements in roof slab.

Table 3
Maximum temperatures recorded in roof slab.

Location	Depth from exposed soffit (mm)	Max. temp (°C)	Time (min)
North (towards the opening)	5	1038	56
	30	575	60
	60	333	72
	90	296	116
	115	253	128
South (towards the opening)	5	771	60
	30	472	68
	60	354	98
	90	371	86
	115	315	106
South (away from the opening)	5	664	62
	30	473	68
	60	287	110
	90	261	110
	115	208	140
North (away from the opening)	5	1062	56
	30	777	60
	60	1305	50
	90	1220	56
	115	1275	56
Centre	5	695	60
	30	412	70
	60	389	64
	90	259	90
	115	*	*

*Could not be recorded due to thermocouple malfunction.

cross section and four across the width of the cross section. The roof slab was provided with a total of 25 thermocouples, 5 each along the depth of the slab at 5 pre-identified locations as shown in Fig. 5(e). All embedded thermocouples were secured in place before the casting of concrete. A total of 301 K-type thermocouples were installed in the test frame for capturing the thermal behaviour of the frame during the heating and cooling regimes of the fire test. The gas temperatures of the designed compartment fire were measured by a network of fifteen thermocouple probes of varying lengths with connection heads. Each thermocouple probe was mineral insulated and positioned vertically at three different plan locations. Each plan location consisted of five thermocouples at elevations of 0.20 m, 0.90 m, 1.60 m, 2.30 m and 2.90 m from the floor level of the compartment. These thermocouples were held in place using thin steel bars to maintain verticality throughout the test. The results from a set of selected sensors have been presented and discussed in the next section. The selected sensors have been identified in Fig. 5(a–e) by placing a red circle around them.

High resolution images of the graduated slab thickness of the test frame were acquired every 8 s using a high resolution digital SLR camera with the intention of creating an independent set of displacement data through image analysis using a Matlab module for Particle Image Velocimetry such as GeoPIV [17]. However, since the test was conducted outdoors, the acquired images had varying lighting conditions which made the image analysis unreliable. Eight data acquisition systems connected to four workstations were used to monitor the real-time output from the sensors. Unique identifications (IDs) were given to each of the sensors to enable programming of the channels of the data acquisition systems. A total of 489 channels were individually programmed to log their respective data (load/temperature/ strain/displacement) every 8 s in synchronization. An uninterrupted power supply was assured throughout the control room by connecting the power to instant power-supply backup, which was finally connected to a 2 kW backup generator set in auto mode.

3. Test results and discussion

Fig. 6(a–c) shows three stages of the experiment, the simulated seismic loading, the fire loading and the residual lateral load capacity test.

3.1. Results of the simulated seismic load test

Fig. 7 shows the hysteretic curve of the test frame, which indicates a maximum displacement of 95 mm in the “push” cycle and 85 mm in the “pull” cycle corresponding to base shears of 316 kN and 267 kN, respectively. Stiffness degradation and pinching effect in the hysteretic loops between successive cycles of loading can be observed in Fig. 7. Although the hysteresis loops continued to remain stable without any significant degradation of strength.

The nomenclature used to identify individual members of the RC test frame is shown in Fig. 8, also showing the north–south orientation of the frame. The test frame was inspected after each cycle of displacement to detect the formation of cracks and monitor their growth. No visually observable cracks were seen up to a lateral displacement of 20 mm corresponding to a roof drift ratio of 0.53%. The first set of cracks developed at the ends of the roof beams oriented along the N–S direction (beam B7) at a lateral displacement of 35 mm (roof drift ratio of 0.92%) corresponding to a base shear of 185 kN. The next set of cracks developed at the ends of the plinth beam B1 also in the N–S direction at the measured lateral displacement of 44 mm corresponding to a base shear of 212 kN. As expected, the flexural cracks occurred earlier and were more pronounced in the beams oriented in the direction parallel to the loading direction. Flexural cracking in the columns was first observed at the junction near the roof beams at a lateral displacement of 31 mm (roof drift ratio of 1.37%). Spalling of concrete was observed at the ends of the roof beams B5 and B7 at a roof drift ratio of about 2%. Widening of cracks was conspicuous in the columns and the plinth beams. It was attempted to maintain the hydraulic pressure in the loading jacks at a constant level when the displacement reached 80 mm (roof drift ratio of 2.11%) corresponding to a base shear of 267 kN (note that the intended displacement was 76 mm). However, due to the limitations of the load-controlled actuators, the actual value of the maximum

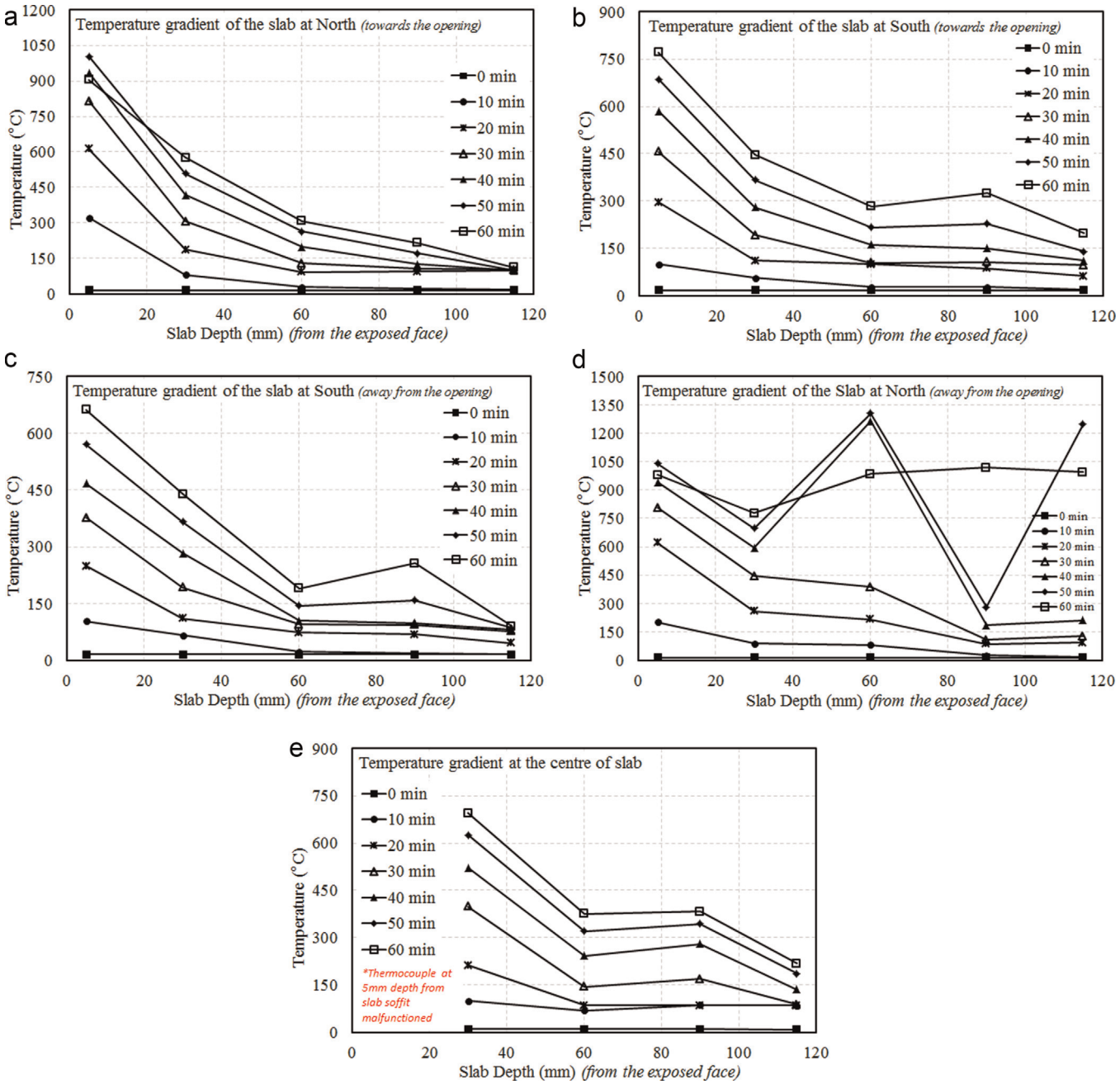

Fig. 14. Variation of temperatures in the roof slab along the depth (a) North (towards the opening), (b) South (towards the opening), (c) South (away from the opening), (d) North (away from the opening) and (e) at the centre.

displacement reached was 95 mm. Flexural cracking, symptomatic of composite action between the RC slab and the roof beams spanning along the N–S direction was noted. After the final loading cycle, these flexural cracks on the roof slab propagated throughout the span from one end to the other in the direction parallel to the direction of loading. The formation of these flexural cracks indicates that a RC roof slab need not necessarily behave as a rigid diaphragm under in-plane loading [18]. Table 2 outlines the sequence of the occurrence of selected cracks in members of the frame that sustained the greatest damage during cycling loading. This table refers to crack locations shown schematically in Fig. 8. The base shear–roof displacement plot for the test frame depicted in Fig. 9 shows no deterioration in the lateral strength of the frame at life safety level of structural performance. Despite the observed inelastic excursions, the test frame did not suffer any significant structural damage. Except for noticeable cracking, no major spalling (loss of big chunks) of concrete or loss of cover (exposing reinforcement) was observed at any location in the test frame at the desired level of mechanical pre-damage.

3.2. Results of the fire test

Real time data recording was facilitated through a synchronized network of data-logging systems which largely performed well during both heating and cooling phases of the fire test. The data from sensors were logged continuously for twelve hours that included the one hour fire and eleven hours of cooling excursion. Detailed results and observations from the fire test are presented in the following sections.

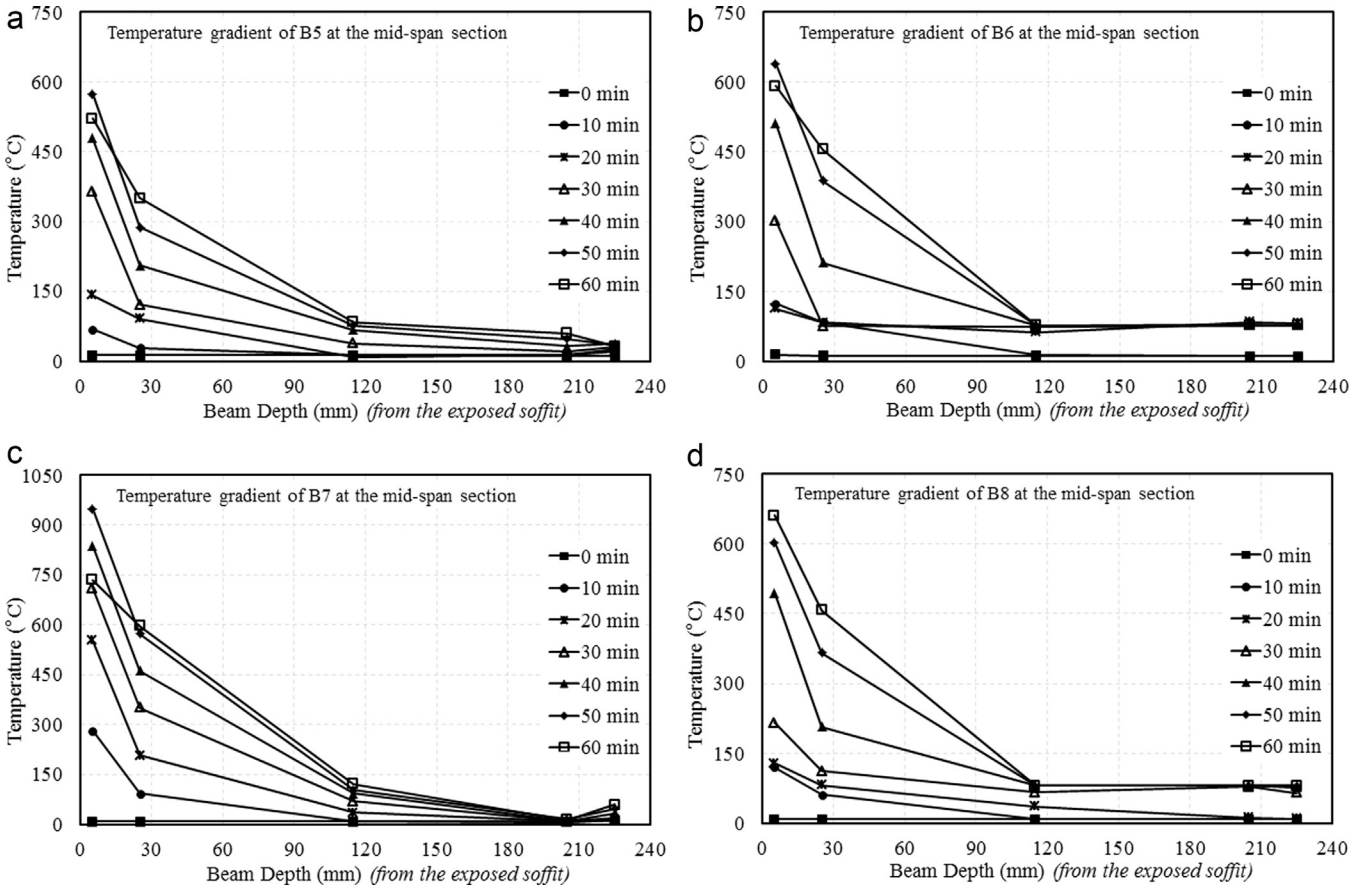

Fig. 15. Typical variation in temperatures in the roof level beams along the depth (a) B5, (b) B6, (c) B7 and (d) B8.

3.2.1. Compartment fire behaviour

Fig. 10(a), (b) and (c) shows the gas temperature history recorded in the fire compartment by three thermocouple trees at different stages of fire: growth (roughly 16 min), fully developed fire stage (1 h) and decay stage (temperatures were measured for over 10 h, 90 min shown). The temperature profiles at five vertical positions inside the compartment, 0.20 m, 0.90 m, 1.6 m, 2.3 m and 2.90 m are shown in each figure at locations A, B and C (as indicated in the inset figure of the compartment). The thermocouples at tree locations A and C at the height of 0.2 m malfunctioned during the test as they were very close to the fire source. The maximum gas temperature recorded inside the compartment during the fire test was 1468 °C. This exceptionally high compartment temperature was attained 62 min after ignition at an elevation of 2.8 m from the floor of the compartment. However, a gas temperature of about 1000 °C was attained within 6 min of ignition as observed from Fig. 10(c). The desired time-temperature behaviour as achieved in mock fire tests was obtained precisely. Flashover occurred between five and seven minutes, after which, the fire advanced to its fully developed stage. As mentioned earlier, the supply of fuel to the pool was terminated after 60 min. However, the fire entered its decay stage once the remaining fuel in the tray had been consumed after approximately 15 min following the termination of fuel supply. Fig. 11 shows a schematic visualisation of the fire in the compartment deduced from observing the flow of smoke and the external flaming. The flow pattern was as expected, however the exceptionally high compartment temperature attained after flashover (the maximum temperatures expected in a compartment fire are usually of the order of 1300 °C) could perhaps be attributed to the very high emissivity of the thick layer of black smoke inside the compartment reaching a depth of over 2 m coupled with a hydrocarbon fuel and a highly insulated compartment lining. This was an unusual feature of this compartment as usually the highest temperatures in compartment fires occur near the top of the compartment. Fig. 10(c) shows that the maximum temperature at the top of the compartment was 1128 °C at 62 min after ignition. The flow pattern within the compartment significantly affected the evolution of temperatures in the structural members and highly non-uniform temperatures were obtained within members that were otherwise at the same height in the compartment. This suggests that the incident heat fluxes at the same elevation were significantly different for different surfaces and were highly dependent on the pattern of the flow of hot gases in the compartment. These differences will be highlighted further in discussing the temperature evolution of various structural members in the following sections.

3.2.2. Behaviour of the frame and individual structural members during the fire test

The first major event to be observed, both visually and audibly, was the spalling (loss of cover concrete at the soffit) of concrete at the roof slab initiating 4–5 min after ignition and continuing for almost 15 min and resulting in the exposure of reinforcement. During this period the compartment temperatures near the roof slab were of the order of 300–400 °C in the front and close to 1000 °C at the back of the compartment where the worst of the spalling was observed, suggesting that a high temperature gradient produces more severe spalling (see Fig. 12). Fire induced spalling is often linked to temperature gradients causing rapid development of pore-pressure in concrete exceeding its tensile strength [19–21], especially in regions of higher compressive stresses. Furthermore, the portions of the roof slab already

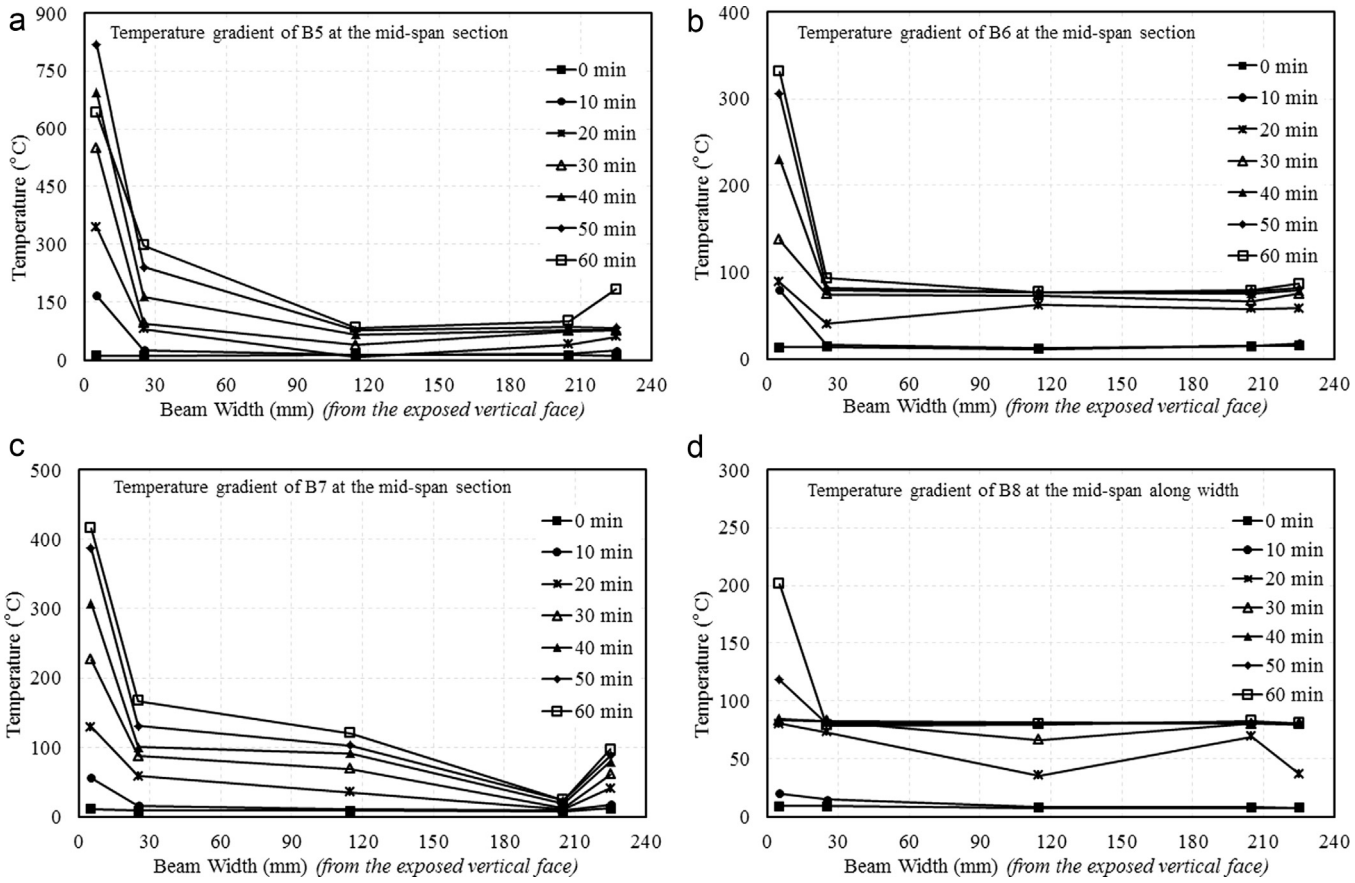

Fig. 16. Typical variation in temperatures in the roof level beams along the width (a) B5, (b) B6, (c) B7 and (d) B8.

damaged during the lateral load test were more vulnerable to spalling compared to the undamaged portions. The loud fire-cracker like sounds which indicated the initiation of spalling suggested that the spalling was of an explosive nature resulting from high pore pressures exacerbated by the fact that the frame had entrapped moisture from the rain earlier in the week before the test. Bazant [22], Ulm [23,24] and Zukov [25] suggest that spalling occurs due to prevented thermal expansion. Careful observation of spalled soffit of the slab suggests high compressive forces were induced in the bottom layers of the roof slab concrete due to the rotational restraint offered by the peripheral beams against thermal bowing (resulting in hogging bending moments across the whole exposed face of the slab). Further high compressive stresses are induced in the layers of concrete near the exposed face which are restrained from expanding thermally by the cooler layers above and ultimately also by the lateral restraint from the peripheral beams. The lack of the spalling around the service holes (made for anchoring thermocouple trees) also indicates that spalling may be influenced by high compressive. Even though compressive stresses exacerbate the severity of spalling, they were also likely to be beneficial to the integrity of the roof slab by aiding compressive membrane resistance (action similar to prestressing). However, spalling remains a very complex phenomenon dependent on parameters such as porosity, permeability, differential thermal expansion between cement paste and aggregate, high moisture content, heating rate and external loads [26] and is not the key focus of the current study. The lack of collapse of the roof slab even after severe spalling means that the effect of thermally assisted compressive membrane action can considerably enhance the load-carrying capacity of the roof slab considerably beyond the calculated flexural resistance. In the later stages of test, i.e., during the growth stage, spalling of concrete and appearance of micro-cracks were observed in beams and columns. In general, the fire induced several surface cracks on all the members which started forming at a temperature of about 600 °C. These cracks further widened at higher temperatures. As observed in the roof slab, the portions of the columns and beams, which suffered greater damage during the simulated earthquake loading, also experienced greater thermal damage.

The end regions of the beams B5 and B7 and columns C3 and C4 suffered minimal damage. The concrete in the soffit of the beam B7 lost its cover at the edge resulting in the exposure of the longitudinal and transverse reinforcement. Visual inspection of the frame was undertaken the 24 h. Unfortunately, the data acquisition of vertical displacements of the roof slab during the fire failed. This was attributed to a transducer malfunctioning under the high temperature environment. However, the post-fire residual vertical displacements of the roof slab were measured using an optical instrument and the schematic is represented in Fig. 13. A maximum residual vertical displacement of 46 mm was recorded in the roof slab after the fire test. Overall, the frame survived the fire exposure without collapse.

3.2.2.1. Roof slab. The maximum temperatures recorded at the five chosen plan locations of the roof slab along the depth are provided in Table 3. It can be observed that near the exposed internal faces at the chosen locations of the slab the temperatures ranged between 664 °C and 1038 °C after about 56–60 min of the start of the fire. The maximum temperatures of 575 °C, 472 °C, 473 °C, 777 °C and 412 °C were observed at a distance of 30 mm from the exposed face i.e. roughly at the cover–core interface at the selected five locations. This shows that the slab experienced relatively higher temperatures throughout its depth compared to the roof beams. A temperature of 1038 °C was recorded at the soffit of the

Table 4
Maximum temperatures recorded in roof level beams.

Member	Direction	Distance from internal surface (mm)	Left section		Mid-span section		Right section	
			Max. temp (°C)	Time (min)	Max. temp (°C)	Time (min)	Max. temp (°C)	Time (min)
B5	**Depth** *(from exposed soffit)*	5	604	52	593	52	784	52
		25	405	58	354	64	527	54
		115	124	168	147	156	123	154
		205	79	316	91	266	84	284
		225	81	220	72	320	76	282
B6	**Depth** *(from exposed soffit)*	5	555	58	658	152	*	*
		25	452	58	455	158	419	60
		115	120	184	163	270	175	148
		205	81	258	96	250	100	282
		225	77	238	82	20	94	294
B7	**Depth** *(from exposed soffit)*	5	902	52	972	52	940	52
		25	507	58	618	56	563	58
		115	172	166	232	128	179	142
		205	117	298	27	718	111	232
		225	111	320	109	286	97	234
B8	**Depth** *(from exposed soffit)*	5	900	58	662	58	662	60
		25	627	60	469	64	395	68
		115	202	144	187	156	124	232
		205	123	282	91	266	99	356
		225	118	296	80	44	93	344
B5	**Width** *(from exposed vertical face)*	5	587	52	840	52	890	52
		25	190	96	329	74	356	74
		205	126	136	192	108	208	100
		225	179	92	230	84	194	100
B6	**Width** *(from exposed vertical face)*	5	169	68	336	56	190	92
		25	175	96	144	154	148	172
		205	99	200	128	266	125	158
		225	101	142	121	166	127	234
B7	**Width** *(from exposed vertical face)*	5	280	60	425	56	279	58
		25	157	164	216	106	150	136
		205	145	206	39	178	114	212
		225	133	206	147	186	98	188
B8	**Width** *(from exposed vertical face)*	5	269	66	*	*	197	78
		25	142	170	146	170	139	176
		205	127	200	122	226	118	254
		225	131	74	106	202	119	176

*Could not be recorded due to thermocouple malfunction.

roof slab at the centre of the span. Temperatures of more than 1200 °C were also noted at depths more than 60 mm from the exposed face in the N–E quarter, but this can be attributed to the loss of concrete and exposure of thermocouples. The temperature variation in the depth of slab is shown in Fig. 14(a–e) at the five plan locations embedded with thermocouples. It was observed that the north half portion of the slab at the rear experienced higher temperatures than the southern half of the slab. Furthermore, in the north half portion, the east side quarter portion had higher temperatures than the western quarter portion. The thermal data and the observations from the visual inspection indicate that the roof slab of the test frame underwent major deterioration under fire in comparison with the other structural components. Despite the considerable damage, no collapse of slab was observed. The slab continued carrying the superimposed loads.

3.2.2.2. Roof level beams. As mentioned earlier, temperatures were recorded at three different sections of all the roof beams, two sections near the joints and the mid-span section. At each of these sections, the temperatures were measured at five locations along both the lateral dimensions of the beam. Fig. 15(a–d) shows variations of temperature with depth from the exposed soffit for all the roof level beams at their mid-span section. The width-wise temperature distribution for the roof level beams from the exposed side face, at the mid-span sections are shown in Fig. 16(a–d). The maximum temperatures attained in the roof beams during the heating stage at various levels along their depths (from exposed soffit) and widths (from exposed vertical face) are given in Table 4. It is observed that the temperatures at the various levels along the depth and across the width of the sections gradually increased with time. The temperatures along the depth of the roof beams B5, B6 and B8, at 5 mm from the exposed soffit were 365 °C, 512 °C and 496 °C after 40 min of the fire exposure. The observed temperatures were high enough to initiate spalling, which correlated with visual observations of beam spalling most which occurred between 30 and 40 min. The average temperature observed at the concrete cover–core interface (25 mm from surface) was 260 °C, however, the temperature at the mid-depth of the beam cross-section at the depth of 115 mm was much lower (80 °C). The temperatures at a depth of 5 mm from the exposed vertical face of B5, B6 and B8 at 40 min were 692 °C, 230 °C and 84 °C, respectively. This indicates that the beam B5 was exposed to higher

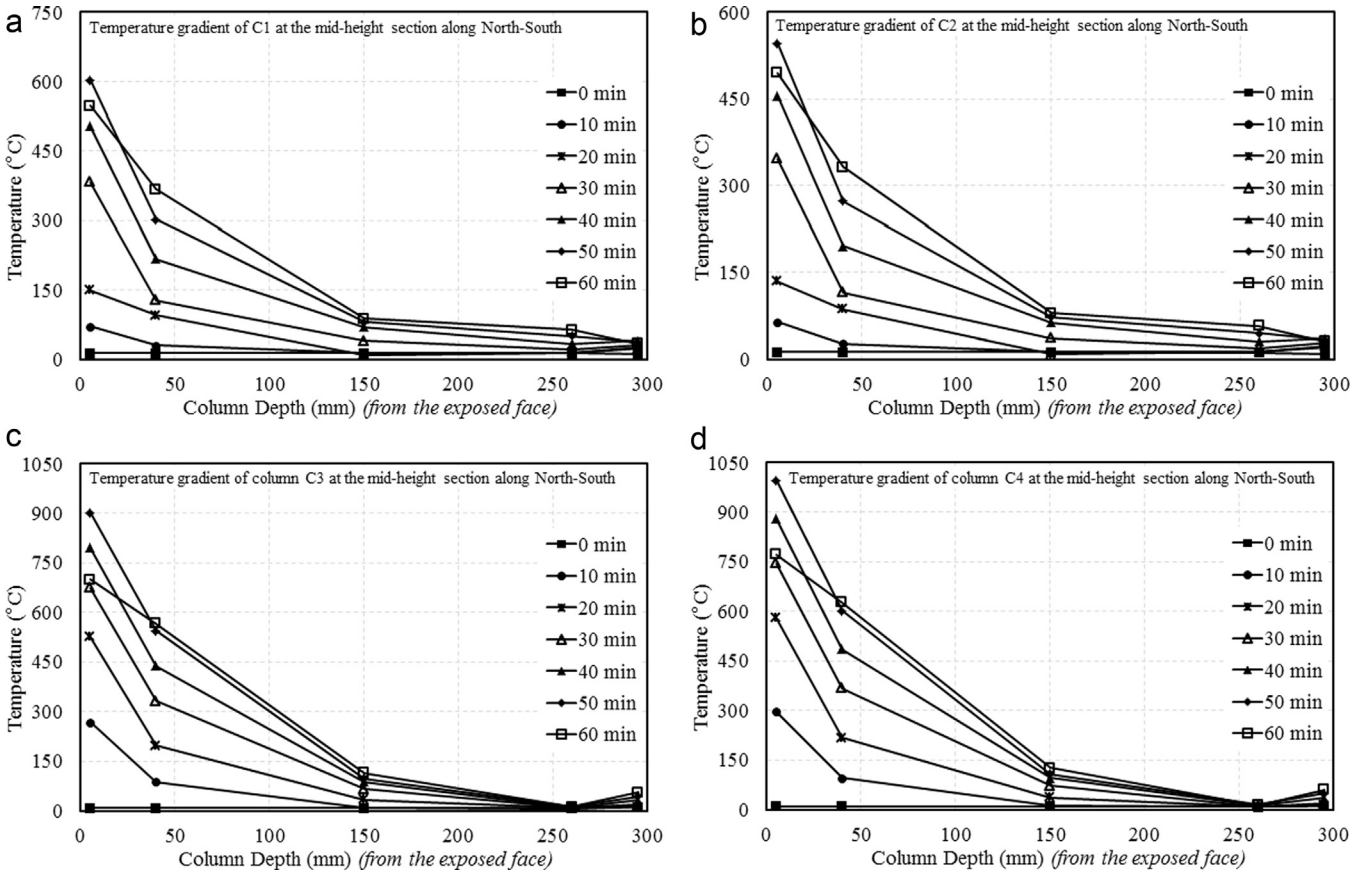

Fig. 17. Typical variation in temperatures in the columns along N–S direction (a) C1, (b) C2, (c) C3 and (d) C4.

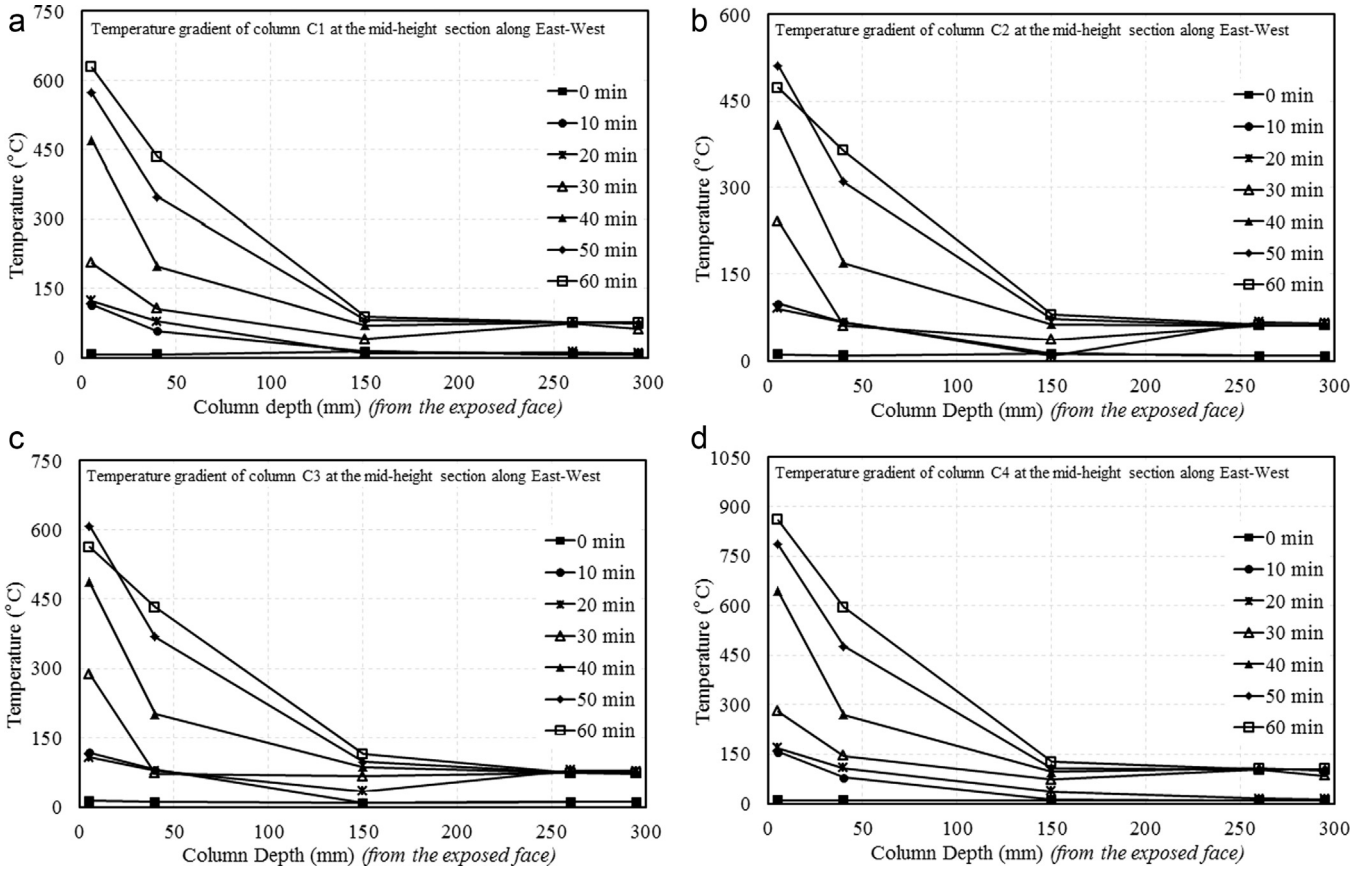

Fig. 18. Typical variation in temperatures in the columns along E–W direction (a) C1, (b) C2, (c) C3 and (d) C4.

Table 5
Maximum temperatures recorded in columns.

Member	Direction	Depth (mm)	Bottom section		Mid-height section		Top section	
			Max. temp (°C)	Time (min)	Max. temp (°C)	Time (min)	Max. temp (°C)	Time (min)
C1	N–S	5	585	58	622	52	725	52
		40	312	62	372	64	486	58
		150	78	148	154	156	149	168
		260	61	260	96	268	95	316
		295	58	278	76	320	97	220
C2	N–S	5	491	62	563	52	862	52
		40	371	64	337	64	579	54
		150	95	116	139	156	135	154
		260	65	232	87	266	92	284
		295	64	238	68	320	84	282
C3	N–S	5	851	42	924	52	947	52
		40	500	64	587	56	532	58
		150	*	*	221	128	180	166
		260	*	*	25	718	123	298
		295	*	*	103	286	117	330
C4	N–S	5	842	58	1021	52	959	52
		40	487	64	649	56	575	58
		150	157	150	244	128	183	142
		260	122	282	28	718	113	232
		295	122	284	114	286	99	234
C1	E–W	5	484	58	629	58	695	60
		40	282	62	446	64	415	68
		260	75	258	86	266	104	356
		295	74	268	76	44	98	344
C2	E–W	5	297	62	527	52	583	58
		40	84	156	364	58	475	58
		260	66	266	77	250	85	258
		295	*	*	65	20	81	238
C3	E–W	5	680	50	625	52	889	54
		40	*	*	432	58	352	58
		260	*	*	91	250	141	54
		295	*	*	78	20	*	*
C4	E–W	5	889	54	861	58	918	58
		40	352	58	610	64	640	60
		260	141	54	118	266	125	282
		295	*	*	104	44	121	296

*Could not be recorded due to thermocouple malfunction.

temperatures on its exposed vertical face than any other roof level beams inside the compartment (eventually reaching a maximum of 890 °C). This is consistent with the fire behaviour as shown in Fig. 11. Beam B7, which was located at the rear of the compartment attained the highest temperatures. At 5 mm depth from the exposed soffit the temperature was 350 °C after 30 min and rose to 840 °C after 40 min of fire exposure (eventually reaching a maximum of 972 °C). This sudden rise in temperature can be attributed to spalling of the corner cover which exposed the thermocouple. Despite high temperatures at the soffit B7 also experienced a low temperature of 120 °C at the mid-depth of the mid-span section. Furthermore, the temperatures measured at the mid-span sections of the roof beams were higher than the temperatures measured near the joints at the corners, where cracks were predominant due to induced seismic damage. This implies that the pre-damage induced at the lateral cyclic loading stage may not have a significant influence on the heat transfer near the corners and certainly much less than the influence of the flow pattern of hot gases in the compartment (Fig. 11) which seem to be the primary governing factor determining the temperature evolution in the structural cross-sections.

3.2.2.3. Columns. The temperatures in the columns were recorded at various sections along their both lateral dimensions designated as N–S direction and E–W direction henceforth. The variations of temperature with the depth of the section for all the chosen sections were then plotted. Some typical plots showing such temperature variations along the depth of the section at the mid-sections of the columns are shown in the Figs. 17(a–d) and 18(a–d), along N–S and E–W directions, respectively. The maximum temperatures attained at different depths at three sections of the columns i.e. near the joints and the mid-height section are given in Table 5. It can be observed that the temperatures decreased along the section with the increase in the distance from the exposed surface, as expected. The temperatures decreased to about 100 °C at a depth of 160 mm along the N–S direction at almost all the sections of the columns. However, in the E–W direction, the rate of decrease of temperature with distance from the exposed surface was lower and therefore the interior regions of columns in E–W direction experienced higher temperatures than in the N–S direction. The top sections of the columns attained higher temperatures than the bottom and mid sections except for the column C4, where the mid-section along N–S direction showed higher temperatures than the end sections. In general, the column C4 experienced the highest temperatures at all the sections followed by columns C3, C2 and C1. Overall, a maximum temperature of 1021 °C was observed on the exposed surface of column C4 at the mid-height section. It was observed that the maximum temperature gradients were greater than 3.5 °C/mm for the portions above the mid height of the column C4. The degradation of concrete was also invariably observed at these locations. Relatively higher thermal damage of top end sections of the columns, especially columns C3 and C4 may also be attributed to the presence of initial lateral load induced cracks and spalling at these locations. However, despite spalling caused by an accelerated heat transfer on pre-damaged surface, the structural stability of the columns remained unaffected after the fire test.

3.2.2.4. Plinth level beams. Fig. 19(a–d) shows the variation of temperatures along the depth at different sections of all the plinth level beams. The temperatures at the exposed surface of beam B1 increased consistently with the duration of the fire with a strong temperature gradient establishing along the depth, with the point furthest from the exposed surface remaining practically unaffected. However, the beam B3 which was located at the rear of the compartment, achieved very high temperatures along its entire depth approximately 30 min into the fire. Similarly the entire section of beam B4 also attained temperatures of over 800 °C at around 40 min. Beam B2 exhibited the most unusual temperature profile, albeit experiencing the lowest temperatures, where the middle section remained relatively cooler than the periphery. Of all the beams only Beam B1 appears to present the expected temperature profile, suggesting that actual heating profile may be significantly affected by highly localised and variable fluxes from the fire, as mentioned earlier. The maximum temperatures obtained at chosen locations of the plinth beams and their corresponding durations are presented in Table 6. The results indicate that the cover concrete of plinth beams experienced considerably high temperatures, which accelerated their deterioration. While the temperatures attained in the core concrete of the plinth beams B1 and B2 were not severe, the plinth beams B3 and B4 attained temperatures of 894 °C and 1037 °C in their core regions, respectively. Overall, a maximum temperature of 1111 °C was recorded on the surface of the plinth beam B4 at its left section.

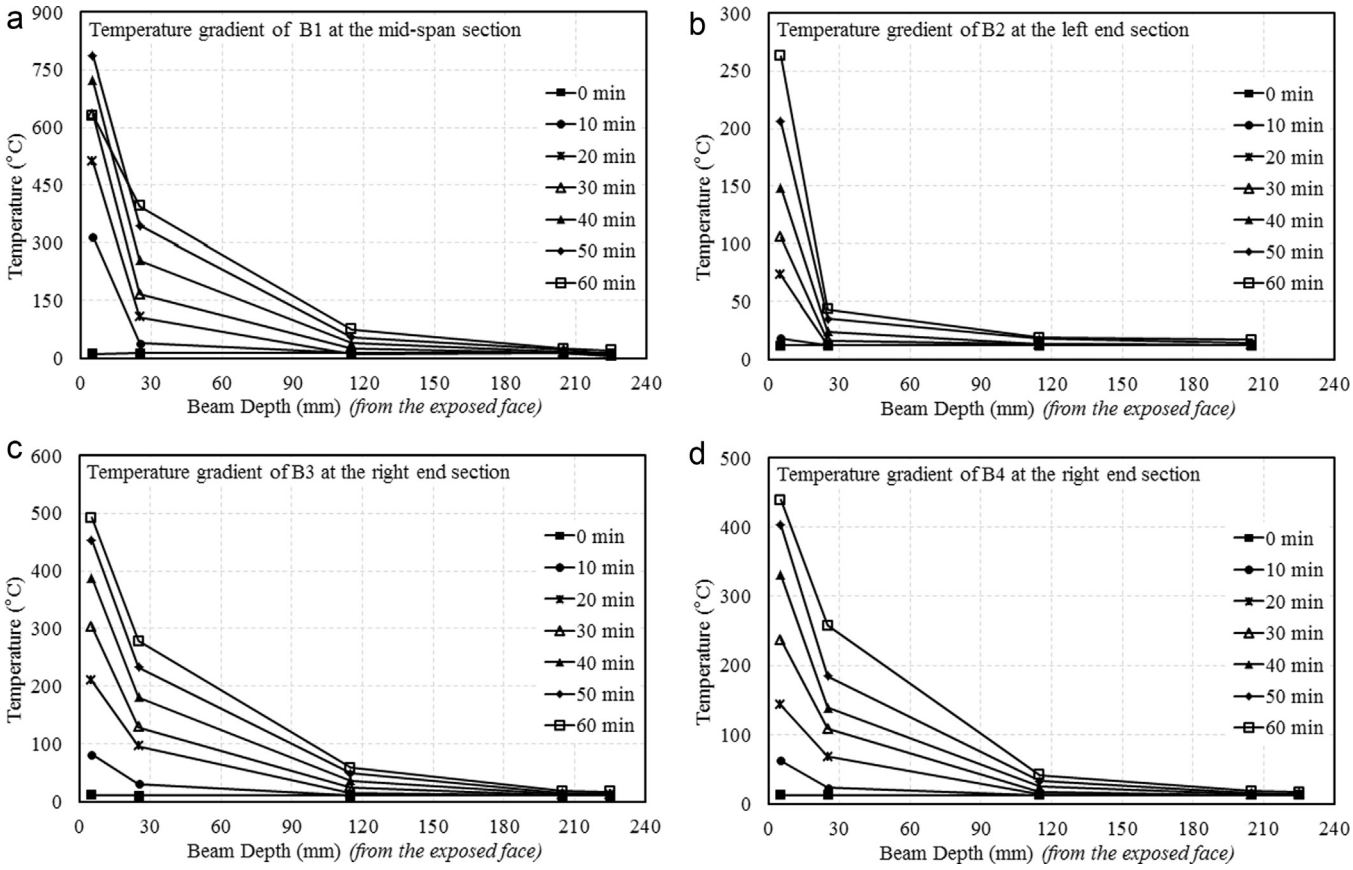

Fig. 19. Typical variation in temperatures in the plinth beams (a) B1, (b) B2, (c) B3 and (d) B4.

Table 6
Maximum temperatures recorded in plinth beams.

Member	Direction	Depth (mm)	Left section		Mid-span section		Right section	
			Max. temp (°C)	Time (min)	Max. temp (°C)	Time (min)	Max. temp (°C)	Time (min)
B1	Depth	5	593	58	827	56	447	62
		25	318	62	397	58	338	64
		115	79	148	116	162	87	116
		205	62	260	90	260	59	232
		225	59	278	88	238	58	238
B2	Depth	5	270	62	508	64	*	*
		25	*	*	608	56	755	55
		115	76	158	351	62	*	*
		205	62	260	*	*	*	*
		225	60	266	358	720	*	v
B3	Depth	5	826	42	829	60	495	58
		25	491	64	865	60	287	64
		115	*	*	894	60	92	152
		205	*	*	*	*	72	280
		225	*	*	*	*	72	284
B4	Depth	5	1111	54	1060	56	448	58
		25	439	58	1064	56	261	62
		115	312	66	1037	56	81	170
		205	177	54	1073	56	70	258
		225	*	*	1076	56	68	268

*Could not be recorded due to thermocouple malfunction.

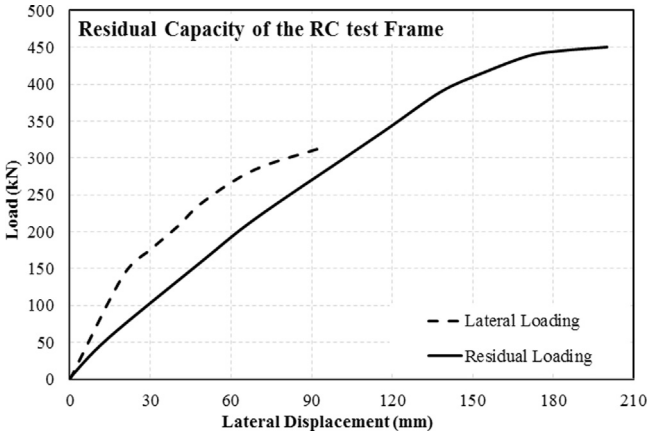

Fig. 20. Comparison of loading envelopes of seismic loading test and residual capacity test.

3.3. Results of the residual capacity test

Uniaxial monotonic lateral loading applied at this stage to the RC test frame was plotted against its corresponding displacement as shown in Fig. 20. The plot is compared with the loading envelope of the cyclic lateral loading in the same direction. The comparison shows a degradation of both strength and stiffness in the test frame after exposure to the simulated seismic and fire loading. An initial loss of 44% in the lateral load resisting capacity was observed at the displacement of 30 mm. At the peak lateral

displacement of 96 mm, applied in the simulated seismic loading stage, 10% degradation in lateral load resisting capacity was observed. It should be noted that the two plots are not strictly comparable as one represents one side of a hysteretic backbone curve and the other represents monotonic pushover. Although numerous cracks and concrete spalling were predominantly observed at displacements beyond 100 mm, the frame showed no sign of collapse. The load was released upon reaching the target displacement of 200 mm. A maximum load of 450 kN was recorded at the target displacement. A residual permanent displacement of 27 mm was observed upon the release of the pushover load.

4. Conclusions

The observations from a realistic compartment fire test on a full-scale RC test frame, which was first subjected to simulated seismic damage, are presented in this paper. Though the failure of the displacement transducers and most of the strain gauges during the fire test hindered the understanding of real time displacements and strains in the frame, the results obtained during the entire test in terms of the residual displacements, temperature distributions and the visual inspections provided substantial useful information on the behaviour of reinforced concrete frame structures subjected to a fire following an earthquake. Within the scope of the present investigation, the following main conclusions may be drawn.

1. FEMA 356 (2000) reports a value of 4% lateral drift at 'collapse prevention' level of structural performance under seismic vulnerability assessment, which was imposed on the RC test frame discussed here. The present test reports that the expected damage condition specified by C1-2 and C1-3 of FEMA is conservative. However, extensive cracks and plastic deformation at probable hinge locations in beams were observed, confirming that the first plastic hinges occurred in beams. Following observations made were contrary to FEMA (in the limited context of this test):

a. Overall damage of the frame was not severe.
b. No large degradation in the overall strength and stiffness was observed.
c. No large permanent drifts were obtained despite inducing a 4% lateral drift.
d. Frame showed no signs of collapse.
e. No extensive spalling were observed in the columns and beams.
f. No buckling of reinforcement were observed.

2. As designed, flashover was achieved within 5–7 min from ignition. An exceptionally high gas temperature of 1468 °C was attained in the middle of the compartment. This can be attributed to a hydrocarbon fuel (kerosene); a very deep smoke layer (over 2 m) resulting in high emissivity; and a highly insulating compartment boundary.
3. The roof slab experienced the greatest fire damage followed by columns, roof beams and plinth beams. The beams and columns positioned at the rear of the compartment experienced greater damage than the ones in the front. The results also show that the position of the opening in the compartment and the resulting movement of fire plume and hot gases have a considerable influence in terms of the evolution of temperatures in the structural sections and therefore the location of damage which may or may not overlap with the locations of damage resulting from the seismic loading. In this test the damage locations did not overlap. There was no influence of pre-damage observed in the RC frame in fire test. Presence of cracking caused by simulated earthquake loading in the RC members did not exacerbate the fire damage as was anticipated. However, damage in beams and columns accelerated the heat transfer through these members. Irrespective of their positions, mid sections of the columns and beams attained higher temperatures than their end sections because of their proximity to the fire source.
4. From the temperature histories recorded inside the compartment, it is evident that the temperature distribution throughout the compartment is non-uniform because of the highly varying surface fluxes imposed by the fire, which confirms that the commonly used uniform compartment temperature assumption in fully developed fires is a crude representation of reality.
5. Because of the unusually deep smoke layer the compartment fire did not conform to the hot upper layer and cool lower layer compartment fire model. The highest temperatures were obtained in the middle third of the compartment and the upper layer showed moderate temperatures. Thus, a three layer pattern was observed in the compartment.
6. This study has generated a database of temperatures and thermal gradients in the various sections of the structural elements of the tested pre-damaged reinforced concrete frame, which provides a useful resource for researchers wishing to validate fire and structural simulations.
7. The better than expected fire resistance of the damaged RC test frame suggests that the Indian Standard recommendations [9,13] for seismic resistant design (particularly the recommendations pertaining to ductile detailing of beam and column reinforcement) are also instrumental in enhancing fire resistance.

Acknowledgements

This work was supported by the UK–India Education and Research Initiative (UKIERI). Authors also acknowledge the Department of Civil Engineering, Indian Institute of Technology Roorkee for the laboratory facilities to carry out the testing of full-scale RC frame.

References

[1] C. Scawthorn, J.M. Eidinger, A.J. Schiff, Fire Following Earthquake, ASCE Publications, Reston, VA, 2005.
[2] C. Scawthorn, W.-F. Chen, Earthquake engineering handbook, CRC press, Boca Raton, FL, 2002.
[3] L.A. Henao, 5 Dead as magnitude-8.2 quake hits northern Chile, ed., Associated Press, Santiago, Chile, AP, 2014.
[4] S. Romero, M. Lacey, Fierce quake devastates Haitian capital, The New York Times, Santo Domingo, Dominican Republic, 2010.
[5] T. UK, Entire Japanese city on fire after earthquake, The Telegraph, Japan, 2011.
[6] G. Ibanez, M. Jarroud, Chile fire toll: 12 dead; 2000 homes destroyed, Associated Press, Chile, AP, 2014.
[7] R. Botting, The impact of post-earthquake fire on the urban environment, University of Canterbury, Canterbury, New Zealand, 1998.
[8] J. Jones, Post earthquake fire results released, Civil Engineering: The Magazine of the American Society of Civil Engineers (2013) (April 16).
[9] BIS, Indian Standard, IS 13920: Ductile detailing of reinforced concrete structures subjected to seismic forces, Bureau of Indian Standards, New Delhi, India, 1993.
[10] BIS, Indian Standard, SP 34: Handbook on concrete detailing and reinforcement, Bureau of Indian Standards, New Delhi, India, 1987.
[11] BIS, Indian Standard, IS 456: Code of practice for plain and reinforced concrete, Bureau of Indian Standards, New Delhi, India, 2000.
[12] BIS, Indian Standard, IS 10262: Concrete mix proportioning-Guidelines, Bureau of Indian Standards, New Delhi, India, 2009.
[13] BIS, Indian Standard, IS 1893(Part 1): General provisions and buildings: Criteria for earthquake resistant design of structures, Bureau of Indian Standards, New Delhi, India, 2002.

[14] FEMA, Prestandard and commentary for the seismic rehabilitation of buildings, Building Seismic Safety Council, Federal Emergency Management Agency, Washington DC, 2000 (FEMA-356).
[15] S. Zhu, J.O. Jirsa, A study of bond deterioration in reinforced concrete beam-column joints, Phil M. Ferguson Structural Engineering Laboratory, University of Texas, Austin, 1983.
[16] P.H. Thomas, A.J.M. Heselden, Fully-developed Fires in Single Compartments: A Co-Operative Research Programme of the Conseil International Du Bâtiment, Building Research Establishment, Fire Research Station, United Kingdom, 1972.
[17] D.J. White, W.A. Take, GeoPIV: Particle Image Velocimetry (PIV) Software for Use in Geotechnical Testing, Technical Report, Cambridge University Engineering Department, Cambridge, UK, 2002.
[18] S.W. Han, O.-S. Kwon, L.-H. Lee, Evaluation of the seismic performance of a three-story ordinary moment-resisting concrete frame, Earthq. Eng. Struct. Dyn. 33 (2004) 669–685.
[19] M.B. Dwaikat, V.K.R. Kodur, Hydrothermal model for predicting fire-induced spalling in concrete structural systems, Fire Saf. J. 44 (4) (2009) 425–434.
[20] Y. Anderberg, Spalling phenomena of HPC and OC in: Proceedings of the International Workshop on Fire Performance of High-Strength Concrete, NIST, Gaithersburg, 1997.
[21] T.Z. Harmathy, Effect of moisture on the fire endurance of building elements, ASTM Special Technical Publication (1965) 74–95.
[22] Z.P. Bazant, M.F. Kaplan, Concrete at High Temperatures: Material Properties and Mathematical Models, Longman Group Limited, 1996.
[23] F.-J. Ulm, P. Acker, M. Lévy, The "Chunnel" fire. II: analysis of concrete damage, J. Eng. Mech. 125 (1999) 283–289.
[24] F.-J. Ulm, O. Coussy, Z.P. Bazant, The "Chunnel" fire. I: chemoplastic softening in rapidly heated concrete, J. Eng. Mech. 125 (1999) 272–282.
[25] V.V. Zhukov, Reasons of explosive spalling of concrete by fire, Beton I zhelezobeton. Concrete and Reinforcement Concrete, , 1976.
[26] M. Kanéma, P. Pliya, A. Noumowé, J. Gallias, Spalling, thermal, and hydrous behavior of ordinary and high-strength concrete subjected to elevated temperature, J. Mater. Civil Eng. 23 (2011) 921–930.